Lattice Monte Carlo for quantum Hall states on a torus

Jie Wang, Scott D. Geraedts, E. H. Rezayi, and F. D. M. Haldane

Phys. Rev. B **99**, 125123 — Published 15 March 2019

DOI: 10.1103/PhysRevB.99.125123

Lattice Monte Carlo for Quantum Hall States on a Torus

Jie Wang,[1] Scott D. Geraedts,[2,1] E. H. Rezayi,[3] and F. D. M. Haldane[1]

[1] *Department of Physics, Princeton University, Princeton NJ 08544, USA*
[2] *Department of Electrical Engineering, Princeton University, Princeton NJ 08544, USA*
[3] *Department of Physics, California State University, Los Angeles, CA 90032, USA*

The Monte Carlo method is very useful for studying various model states proposed for the fractional quantum Hall systems. In this paper, we introduce a lattice Monte Carlo method based on an exact lattice formalism for quantum Hall problems defined on a torus. This "lattice representation" is applied to study the many body Berry phase of the Composite-Fermi liquid phase in a half-filled Landau level. The Monte Carlo result agrees with the exact numerical result found on small systems sizes, and is consistent with the prediction from the Dirac fermion low energy effective theory. Many other aspects of other model states, including the structure factor, Coulomb energy and particle-hole symmetry, are studied and discussed.

I. INTRODUCTION

Strongly interacting electrons in high magnetic field exhibit rich physical properties. Numerical Monte Carlo studies of quantum Hall model wavefunctions have long been an important tool in understanding quantum Hall physics. Quantities such as the ground-state energies, quasiparticle gaps, density-density correlation functions (structure factors), quasiparticle statistics and more have all been calculated using these methods [1–8]. Like many numerical methods, these Monte Carlo studies are limited in the system sizes they can access, and methods to increase these system sizes can allow for new measurements and lead to new physical insights.

The torus geometry has been one of the most useful platforms for studying Fractional Quantum Hall (FQH) states [9, 10]. The translation group of a charged particle in a magnetic field on a torus has a rich structure which has allowed a deeper understand of topological properties. Recently, one of us has shown that instead of the continuous formalism, a rigorous finite "lattice representation" [11] can be built on the torus, using the subgroup of discrete translations compatible with the magnetic translation group in this compact geometry. One application of this lattice formalism is the lattice Monte Carlo method presented here.

The composite Fermi liquid (CFL) state that can occur at Landau level (LL) filling $\nu = 1/q$ (q is even) is one of the interesting phases that two dimensional interacting electrons in magnetic field can exhibit. The CFL phase has been understood in a number of ways, such as the Halperin-Lee-Read (HLR) theory [12] where the composite fermions (physical electrons bound to q "flux quanta" or vortices) form a Fermi sea. At LL filling $\nu = 1/2$, electrons interacting via two-body interactions have an exact particle-hole symmetry, while it is not obvious how HLR theory is consistent with this symmetry [13–19]. This motivated Son [20] to consider an alternative effective field theory where the composite fermions are neutral Dirac fermions, and the particle-hole transformation acts as a time-reversal transformation on these Dirac fermions. In the Dirac picture, the Fermi sea has a singular point at its center, with a Berry flux of π, giving a Z_2 Berry phase factor of -1 for an adiabatic path in momentum space where a single composite fermion encircles the singular point an odd number of times. Such a π Berry phase was later indirectly confirmed in a recent density matrix renormalization group study [21].

In the work described here, we directly compute the CFL Berry phase and Berry curvature by transporting composite fermions along different closed paths. The Monte Carlo computation uses the lattice representation presented here and is based on a determinant variational model wavefunction [22–24] that is found to describe the CFL phase very well when the (discrete) variational parameter, the composite fermion configuration, is clustered to form a compact Fermi sea [25]. Our lattice Monte Carlo result for the Berry phase of the many-particle wavefunction agrees with a study (using much smaller system sizes) based on exact numerical methods [25], which our lattice Monte Carlo study confirms using much larger sizes.

In this work, we will show why a lattice representation can be built on the torus, how the lattice-based Monte Carlo method is able to significantly speed up calculations, and compute a variety of physical interesting properties including the many body Berry phase in the CFL state, the structure factor, pair-amplitude and Coulomb energy for various model states. We begin in Section II with a pedagogical review of the FQH physics with the emphasis on the guiding centers and the translation symmetry, and finally introduce the lattice representation and the lattice Monte Carlo method. In the subsequent sections we provide some examples of calculations which can be performed using this new Monte Carlo method. In Section III, we compute Berry phases for quasiparticles in the Laughlin state, as well as the Berry phase acquired when moving composite fermions around the Fermi sea in a CFL state. In Section IV, we compute structure factors for various quantum Hall states at very large sizes, and introduce a Brillouin zone truncation method to further improve the Monte Carlo efficiency. Finally in Section V, we show how the Monte Carlo method can be used to evaluate the particle-hole

symmetry of wavefunctions.

II. LATTICE MONTE CARLO METHOD

In this section, we will introduce our basic notation, and provide a brief review of the guiding center physics and translational symmetry on the torus. Both of these played an important role in the development of the "Lattice representation" [11].

A. Review of Guiding Center Physics

A generic quantum Hall problem is formed by a 2D electron gas (2DEG) in a high magnetic field. The Hamiltonian that describes this system contains a kinetic term H_0 and an interaction term V,

$$H = H_0 + \sum_{i<j} V(\boldsymbol{r}_i - \boldsymbol{r}_j), \quad H_0 = \sum_i \epsilon(\boldsymbol{\pi}_i). \tag{1}$$

where $\epsilon(\boldsymbol{p})$ is the single body dispersion and $\boldsymbol{\pi}_i = \boldsymbol{p}_i - e\boldsymbol{A}(\boldsymbol{r}_i)$ is the gauge invariant dynamical momentum. This momentum satisfies $[\pi_{i,a}, \pi_{j,b}] = i\hbar\delta_{i,j}\epsilon_{ab}l_B^{-2}$ where $l_B = \sqrt{eB/\hbar}$ is the magnetic length and ϵ_{ab} is the 2D anti-symmetric symbol (which is odd under the antiunitary time-reversal and particle-hole-conjugation (within a LL symmetries). Here the subscripts i, j label different electrons while spatial indices a, b label directions. With this convention, the cyclotron motion of the electron is clockwise, and the "magnetic area" occupied by one flux quanta is $2\pi l_B^2$.

The electron positions (displacements from an arbitrary origin on the 2D plane) $\{\boldsymbol{r}_i\} = \{r_i^a \boldsymbol{e}_a\}$ can be reorganized to two independent sets,

$$r_i^a = R_i^a + \bar{R}_i^a. \tag{2}$$

where $\bar{R}_i^a \equiv -l_B^2\epsilon^{ab}\pi_{i,b}$ describes the electrons orbital motion and R_i^a is the guiding center coordinate which is the center of classical cyclotron motion. (Note that our formalism distinguishes components of displacements, which have upper indices, from those of derivatives, which have lower indices, as the Euclidean metric $\delta_{ab} = \boldsymbol{e}_a \cdot \boldsymbol{e}_b$ has no role in the physics other than to define a Cartesian coordinate system, and the common assumption that introduces it by postulating a Newtonian form $\varepsilon(\boldsymbol{\pi}) = \frac{1}{2}m^{-1}\delta^{ab}\pi_a\pi_b$ will not be made here; in general there is no place for the the Euclidean metric in the the physics of electrons moving in a fixed crystalline background.) The algebras of these new coordinates are $[\bar{R}_i^a, \bar{R}_j^b] = il_B^2\epsilon^{ab}\delta_{i,j}$, $[R_i^a, R_j^b] = -il_B^2\epsilon^{ab}\delta_{i,j}$ and $[\bar{R}_i^a, R_j^b] = 0$. The kinetic part of the Hamiltonian, H_0, produces LL quantization. In the limit where the LL energy-splitting is much larger than the interaction energy, the wavefunction can be written as an *unentangled product* of the Landau orbit part and the guiding center part

$$|\psi_n\rangle = |\psi_n^{LO}\rangle \otimes |\psi^{GC}\rangle. \tag{3}$$

Here $|\psi_n^{LO}\rangle$ is the Landau orbit part, where n indicates that the system is in the n_{th} LL. $|\psi^{GC}\rangle$ is the guiding center part of the wavefunction. The LL part of the wavefunction can be projected out, leaving the problem essentially a degenerate perturbation problem within a specific LL described by a set of non-commutative interacting guiding center coordinates R_i^a [26],

$$H = \sum_{i<j} V(\boldsymbol{R}_i - \boldsymbol{R}_j). \tag{4}$$

Here the "guiding-center interaction potential" $V(\boldsymbol{r})$ depends not only on the "bare" Coulomb interaction, but also on the "form-factor" of the LL into which it is projected. It is an extremely smooth function, with a rapidly-decaying Fourier transform due to the Gaussian-like form-factor, which means that the expansion of $V(\boldsymbol{r} + \delta\boldsymbol{r})$ in powers of δr^a is absolutely convergent for all $\boldsymbol{r}$. This property ensures that, as a function of non-commuting variables, $V(\boldsymbol{R}_i - \boldsymbol{R}_j)$ is well-defined.

In the following we will work on a torus with primary translations $\boldsymbol{L}_1$ and $\boldsymbol{L}_2$, which contains flux $2\pi N_\phi = |\boldsymbol{L}_1 \times \boldsymbol{L}_2|$. Model wavefunctions on the torus contain an implicit "complex structure", which describes a mapping between the torus and the complex plane: $z \equiv w_a x^a$. A complex structure is defined by a unimodular (unit determinant) Euclidean-signature metric through $g_{ab} = w_a^* w_b + w_a w_b^*$ and $i\epsilon_{ab} = w_a^* w_b - w_a w_b^*$. The complex lattice is then $\mathbb{L} \equiv \{mL_1 + nL_2\}$, $L_i = w_a \boldsymbol{L}_i^a$, and the quantization condition translates to $L_1^* L_2 - L_1 L_2^* = 2\pi i N_\phi$. The metric g_{ab} is a continuously-variable parameter of the model wavefunction that generally parameterizes the shape of "flux attachment", or a correlation hole around each particle. If the interaction $V(\boldsymbol{r})$ has a rotational symmetry, so $V(\boldsymbol{r}) = f(g^0_{ab} r^a r^b)$, the natural choice for g_{ab} is g^0_{ab}, but otherwise g_{ab} should be chosen to minimize the variational energy of the model wavefunction.

The symmetry group on a torus in a magnetic field is the magnetic translation group, whose group elements are $t(\boldsymbol{d}) \equiv e^{i\boldsymbol{d}\times\boldsymbol{R}}$, where $\boldsymbol{d}$ is a vector in real space. The $t(\boldsymbol{d})$ satisfy the Heisenberg algebra

$$t(\boldsymbol{d} + \boldsymbol{d}') = t(\boldsymbol{d})t(\boldsymbol{d}')e^{\frac{i}{2}\boldsymbol{d}\times\boldsymbol{d}'}. \tag{5}$$

A periodic translation must leave the wavefunction invariant up to a phase:

$$t(L)\psi(z) = \eta_L^{N_\phi} e^{i\phi_L}\psi(z), \tag{6}$$

where $\eta_L = 1$ if $\frac{1}{2}L \in \mathbb{L}$, $\eta_L = -1$ otherwise. The phase ϕ_L is a boundary condition parameter, that has no significance if the system is translationally invariant, when it can conveniently be set to zero. Translating the wavefunction by a non-integer multiple of $\boldsymbol{L}/N_\Phi$ would change the boundary condition and this imposes the the condition that $d \equiv w_a \boldsymbol{d}^a$ is quantized with discrete values $mL_1/N_\phi + nL_2/N_\phi$.

Since wavefunctions on a torus are quasiperiodic, they are naturally expressed in terms of various elliptic functions. In this work the elliptic function we will use is what we call the "modified Weierstrass sigma functions" $\sigma(z)$ [27], which we then multiply by a Gaussian. This function, which we will call $f(z) = \sigma(z)e^{-\frac{1}{2N_\phi}zz^*}$, is the building block of the model wavefunctions in Section III.

Combining all the properties described above, we can now explicitly write model wavefunctions. We start with the simplest case, the wave function for a single electron, which is also the building block for many body wavefunctions:

$$\psi(z,\{\alpha\}) = \prod_i^{N_\phi} f(z-\alpha_i)e^{\frac{1}{2N_\phi}(\alpha_i^* z - \alpha_i z^*)}. \quad (7)$$

Since this wavefunction is essentially holomorphic [it is easily verified that it is a holomorphic function times a Gaussian by substituting $f(z) = \sigma(z)e^{-\frac{1}{2N_\phi}zz^*}$], it is uniquely determined given its zeros $\{\alpha_i\}$. Under a translation around the torus the wavefunction becomes:

$$t(L)\psi(z,\{\alpha\}) = \eta_L^{N_\phi} e^{L^*\bar{\alpha} - L\bar{\alpha}^*}\psi(z,\{\alpha\}). \quad (8)$$

where $\bar{\alpha} = \sum_i \alpha_i/N_\phi$ is the average of all zeros. By comparison with Eq. (6) we see that the $\bar{\alpha}$ sets the boundary conditions of the wavefunction. As noted previously, we will use the boundary condition: $\sum_i \alpha_i = 0 \bmod L$.

Note we are not limiting ourselves to the lowest LL by using holomorphic wavefunctions. Holomorphic functions are just representations of guiding center states and are generic to any LL; the "wavefunction" is really a representation of a Heisenberg state of the guiding center projected into any LL [11, 27],

$$\Psi(z) \equiv F(z)e^{-\frac{1}{2}z^*z} \mapsto F(a^\dagger)|0\rangle, \quad a|0\rangle = 0, \quad (9)$$

where $a^\dagger = w_a^* R^a$.

B. Lattice Representation and Monte Carlo

A number of useful calculations (*e.g.*, overlaps, operator expectation values) can be made by integrating over the positions of all electrons in a model wavefunction. As shown in Ref. 11, overlap of two holomohrpic torus wavefunctions can be replaced by an exact lattice sum. In this short section, we start with an introduction to the "lattice representation" with an emphasis on its operator form, and then describe how these calculations can be performed using the Metropolis-Hastings algorithm [28, 29]. We will focus on two-body operators since these are used in calculations of important quantities such as the energy or the structure factor.

1. Lattice Representation Operator Form

The key advantage of our method lies in the fact that continuous integrations can be replaced with lattice sums on the torus in an exact way [11]. We are interested in knowing the mean value of a translationally invariant two-body operator $\sum_{i<j} O(\boldsymbol{x}_i - \boldsymbol{x}_j)$, averaged by states $|\psi_{n,1}\rangle$ and $|\psi_{n,2}\rangle$ in the n_{th} LL, which by definition is given by continuous integration,

$$\langle\psi_{n,1}|\hat{O}|\psi_{n,2}\rangle \quad (10)$$
$$\equiv \prod_k^{N_e}\int d^2\boldsymbol{x}_k\ \psi_{n,1}^*(\{\boldsymbol{x}\})\psi_{n,2}(\{\boldsymbol{x}\})\sum_{i<j}O(\boldsymbol{x}_i-\boldsymbol{x}_j).$$

where we use $\hat{O}$ to represent an operator and $O(\boldsymbol{x})$ to denote its coordinate representation.

In fact, such calculation can be replaced by a lattice summation for operator $\hat{O}^{Lat}$, which we call as the "lattice representation" of $\hat{O}$,

$$\langle\psi_{n,1}|\hat{O}|\psi_{n,2}\rangle = C\langle\psi_{0,1}|\hat{O}^{Lat}|\psi_{0,2}\rangle_{Lat}. \quad (11)$$

where the symbol $\langle|...|\rangle_{Lat}$ means lattice summation, defined as follows,

$$\langle\psi_{0,1}|\hat{O}^{Lat}|\psi_{0,2}\rangle_{Lat} \quad (12)$$
$$\equiv \prod_k^{N_e}{\sum_{\boldsymbol{x}_k}}'\ \psi_{0,1}^*(\{\boldsymbol{x}\})\psi_{0,2}(\{\boldsymbol{x}\})\sum_{i<j}O^{Lat}(\boldsymbol{x}_i-\boldsymbol{x}_j).$$

In the above, $\sum'_{\boldsymbol{x}}$ means summing over the $N_\phi \times N_\phi$ evenly spaced lattice $\boldsymbol{x} \in \{(m\boldsymbol{L}_1 + n\boldsymbol{L}_2)/N_\phi | m,n \in \mathbb{Z}\}$. The constant C is fixed once the $N_\phi \times N_\phi$ lattice is chosen, and it is not important since it is always canceled out by wavefunction normalization factors. In the following, we want to derive the expression of $O^{Lat}(\boldsymbol{x}) \equiv \langle\boldsymbol{x}|\hat{O}^{Lat}|\boldsymbol{x}\rangle$.

Note that in Eq. (11) we wrote states on the right side with LL index $n = 0$. By doing this, we mean that the physical problem in an arbitrary LL can be solved by using the lowest LL wavefunctions as a technical device.

The translation group plays the central role in the derivation of the lattice representation. To see this, we start by finding the effective interaction potential for guiding centers. First, do a Fourier expansion for $\hat{O}$, yielding,

$$\langle\boldsymbol{x}_{ij}|\hat{O}|\boldsymbol{x}_{ij}\rangle \equiv O(\boldsymbol{x}_i-\boldsymbol{x}_j) = \frac{1}{2\pi N_\phi}\sum_{\boldsymbol{q}}O(\boldsymbol{q})e^{i\boldsymbol{q}\cdot(\boldsymbol{x}_i-\boldsymbol{x}_j)}.$$

where the unprimed sum $\sum_{\boldsymbol{q}}$ sums all discrete $\boldsymbol{q}$ allowed by boundary condition.

Now we split up the coordinate and wavefunction into "Landau orbit" and "guiding center" parts using Eqs. (2) and (3). This allows us to write it as,

$$\langle\psi_{n,1}|\hat{O}|\psi_{n,2}\rangle = \quad (13)$$
$$\frac{1}{2\pi N_\phi}\sum_{\boldsymbol{q}}\sum_{i<j}O(\boldsymbol{q})f_n^2(\boldsymbol{q})\langle\psi_1^{GC}|e^{i\boldsymbol{q}\cdot(\boldsymbol{R}_i-\boldsymbol{R}_j)}|\psi_2^{GC}\rangle.$$

where $f_n(\boldsymbol{q})$ is the LL "form factor" defined as:

$$f_n(\boldsymbol{q}) \equiv \langle\psi_n^{LO}|e^{i\boldsymbol{q}\cdot\bar{\boldsymbol{R}}}|\psi_n^{LO}\rangle = L_n(\tfrac{1}{2}\boldsymbol{q}^2l_B^2)e^{-\frac{1}{4}\boldsymbol{q}^2l_B^2}. \quad (14)$$

A key observation is that $e^{i\boldsymbol{q}\cdot\boldsymbol{R}_i}$ in Eq. (13) is nothing but the magnetic translation operators, which satisfy the Heisenberg algebra Eq. (5). Note that the periodic translation ($\boldsymbol{q} \in \mathbb{L}$) leaves the state invariant up to a phase factor Eq. (6). We thus can break up the sum over $\boldsymbol{q}$ into a sum over the first Brillouin zone [indicated by the prime on the sum $\sum'$], and the sum over the rest of $\boldsymbol{q}-$space included in $O^{GC}(\boldsymbol{q})$. Now Eq. (13) becomes,

$$\langle\psi_{n,1}|\hat{O}|\psi_{n,2}\rangle = \frac{1}{2\pi N_\phi}\sum_{\boldsymbol{q}}{}' \sum_{i<j} O^{GC}(\boldsymbol{q})\langle\psi_1^{GC}|e^{i\boldsymbol{q}\cdot(\boldsymbol{R}_i-\boldsymbol{R}_j)}|\psi_2^{GC}\rangle. \tag{15}$$

where $O^{GC}(\boldsymbol{q})$ is the interaction defined only in the first Brillouin zone but it includes all other short range interactions exactly. Because of the exponential tail of the form factor, the numerical value of $O^{GC}(\boldsymbol{q})$ is dominated by the part of $O(\boldsymbol{q})$ in the first Brillouin zone,

$$\begin{aligned} O^{GC}(\boldsymbol{q}) &= [O(\boldsymbol{q})f_n^2(\boldsymbol{q})]_c \\ &\equiv \sum_{\boldsymbol{q}'} O(\boldsymbol{q}+\boldsymbol{q}'N_\phi)f_n^2(\boldsymbol{q}+\boldsymbol{q}'N_\phi). \end{aligned} \tag{16}$$

Eqs. (15) and (16) are close to the final expression of lattice representation $O^{Lat}(\boldsymbol{x})$ that satisfies Eq. (11). As the central result in this section, it is,

$$O^{Lat}(\boldsymbol{x}) = \frac{1}{2\pi N_\phi}\sum_{\boldsymbol{q}}{}' \frac{O^{GC}(\boldsymbol{q})}{|[f_0(\boldsymbol{q})]_{N_\phi}|^2} e^{i\boldsymbol{q}\cdot\boldsymbol{x}}. \tag{17}$$

We give more details of the derivation in the Appendix. They symbol $[...]_{N_\phi}$ used in Eq. (17) denotes a "compactification", defined as the following for arbitrary operator $\chi(\boldsymbol{q})$,

$$\begin{aligned} [\chi(\boldsymbol{q}_{mn})]_{N_\phi} = \sum_{k,l} &\chi(\boldsymbol{q}_{mn}+\boldsymbol{q}'_{kl}N_\phi)e^{i(k\phi_1+l\phi_2)} \\ &\times (-1)^{ml-nk+N_\phi(kl+k+l)}. \end{aligned} \tag{18}$$

where $\phi_{1,2}$ is the boundary condition $t(\boldsymbol{L}_{1,2})|\psi\rangle = -e^{i\phi_{1,2}}|\psi\rangle$, $\boldsymbol{q}_{mn} \equiv (m\boldsymbol{L}_1 + n\boldsymbol{L}_2)/(N_\phi l_B^2)$. Due to the exponential decay of the form factor, the compactification used in Eq. (17) is effectively constrained in the first Brillouin zone. Note that when $O(\boldsymbol{x})$ is identity, we recover the central result in [11]: the expression of the overlap of wavefunctions can be replaced by a lattice summation.

At this stage, we make some comments on the result. The emergence of the $\boldsymbol{q}-$space Brillouin zone in Eq. (15) is purely a consequence of the translation group, and this indeed implies a real space lattice structure: states and operators can be formulated on the lattice. Since we worked out the whole problem in the guiding center space, the lattice representation is generic to any LL; the lowest LL wavefunction in Eq. (11) is not special, but serves just as a technical device to solve the problem in a generic LL. Furthermore, in some cases when the two body operator $O(\boldsymbol{q})$ is divergent if it is put on the infinite plane, their lattice representations are convergent. As can be seen from Eq. (17), the numerator and denominator are regularized by Gaussian factor first and are compactified separately, making the potential convergent. This is not surprising, since the lattice provides a natural regularization. We will see this again when working on the high LL Coulomb energy and pair-amplitude.

2. *Lattice Monte Carlo*

To set up the the Metropolis algorithm, using the lattice representation, we rewrite expectation value as:

$$\begin{aligned} &\frac{\langle\psi_1|\hat{O}|\psi_2\rangle}{\sqrt{\langle\psi_1|\psi_1\rangle\langle\psi_2|\psi_2\rangle}} \\ &= \frac{[\sum'|\psi_1(\boldsymbol{x})|^2\cdot O^{Lat}(\boldsymbol{x})\cdot\psi_2(\boldsymbol{x})/\psi_1(\boldsymbol{x})]/\sum'|\psi_1(\boldsymbol{x})|^2}{\sqrt{[\sum'|\psi_1(\boldsymbol{x})|^2\cdot|\psi_2(\boldsymbol{x})/\psi_1(\boldsymbol{x})|^2]/\sum'|\psi_1(\boldsymbol{x})|^2}}. \end{aligned} \tag{19}$$

We obtained this equation by writing the overlaps as sums over all positions of the coordinates, and then multiplying the numerator and denominator by $|\psi_1(\boldsymbol{x})|^2/[|\psi_1(\boldsymbol{x})|^2\sum'_{\boldsymbol{x}'}|\psi_1(\boldsymbol{x}')|^2]$. In the above, $\sum'$ sums over $\boldsymbol{x} = \{\boldsymbol{x}_1, ...\boldsymbol{x}_{N_e}\}$ which represents a point in the many body coordinate space. All $\boldsymbol{x}_i$ live on the lattice, therefore $\boldsymbol{x}$ is $N_\phi^{2N_e}$ dimensional. Writing the overlap in this way makes it clear that both the numerator and denominator can be computed using a Monte Carlo algorithm with Metropolis weight $|\psi_1|^2$.

In Table I, we test our Monte Carlo method by computing the Coulomb energy, $O(\boldsymbol{x}) \to V(\boldsymbol{x}) = 1/|\boldsymbol{x}|$, for the Laughlin wavefunction at $\nu = 1/3$ in the first few LLs. The tables shows the exact energies and those determined by Monte Carlo, for a few different system sizes. The energy includes the "Madelung energy" [30, 31], which is due to an electron's interaction with periodic copies of itself. The fact that our results agree to several digits (limited only by the statistical error of the Monte Carlo) is a confirmation that our lattice Monte Carlo does give correct results. To the best of our knowledge, the first Monte Carlo calculation of Laughlin $\nu = 1/3$ lowest LL Coulomb energy was done in [3] for up to 144 electrons. Using the lattice method presented here, and by virtue of a modern computer, we can do much larger sizes (*e.g.* for 200 electrons the energy -0.40969 ± 0.00002 can be computed within 100 CPU hours). For higher LLs $n > 1$, we find very large statistical errors which prevent us from obtaining the energy directly through the Monte Carlo. The cause of this problem (and a solution which improves the Monte Carlo efficiency significantly) are provided in Section IV.

III. BERRY PHASE

In this section we use the Monte Carlo method to calculate the Berry phases acquired when various quasiparticles are moved around a closed path. We will start from an easy case of moving a quasi-hole in the Laughlin

$n=0$		
N_e	Exact	Monte Carlo
4	-0.414171	-0.414172 ± 0.000001
5	-0.412399	-0.412397 ± 0.000001
6	-0.411583	-0.411585 ± 0.000001
$n=1$		
N_e	Exact	Monte Carlo
4	-0.339105	-0.33907 ± 0.00005
5	-0.334207	-0.33421 ± 0.00004
6	-0.331879	-0.33190 ± 0.00007
$n=2$		
N_e	Exact	Monte Carlo
4	-0.280537	-0.278 ± 0.004
5	-0.278052	-0.280 ± 0.005
6	-0.274849	-0.26 ± 0.01
$n=3$		
N_e	Exact	Monte Carlo
4	-0.257681	-0.26 ± 0.09
5	-0.254155	-0.4 ± 0.2
6	-0.251042	-0.7 ± 0.9

TABLE I: Comparison of exact and Monte Carlo energies for the Laughlin wavefunction at ν=1/3. The agreement between the two, limited only by statistical error, is a confirmation that our lattice Monte Carlo is correct. For n>1 the statistical error is large. The cause and solution of this problem are described in Section IV.

state. This serves as an example of a Berry phase calculation and demonstrates that our Monte-Carlo method works. Then we will proceed to the gapless CFL phase. The Berry phase obtained by the composite fermions as they move around the Fermi surface has attracted recent interest due to its relationship with various particle-hole symmetric theories of the CFL [17, 18, 20, 21, 25, 32–35].

A. Laughlin-hole Berry Phase

As a first example we move one quasi-hole in the $\nu = 1/q$. In this section, we use q as the inverse of the filling fraction. Laughlin state around an area A in which no other quasiholes are present, and the particle density is uniform. Since the quasi-hole is charged and there is a magnetic field passing through the system, the quasi-hole should pick up a Berry phase of $2\pi A/q$. Before doing the Berry phase calculation, we first review the Laughlin and Laughlin-hole wavefunction on the torus.

On the infinite plane, Laughlin's $\nu = 1/q$ wavefunction [2] is given by $\prod_{i<j}(z_i - z_j)^q e^{-\frac{1}{2l_B^2}\sum_i z_i z_i^*}$. The torus generalization of it [9, 10] is,

$$\Psi(\{\alpha\}) = \prod_{i<j}^{N_e}[f(z_i - z_j)]^q \prod_{k=1}^{q} f(Z - \alpha_k). \qquad (20)$$

where $Z = \sum_i^{N_e} z_i$ is the center-of-mass coordinate. The first term of Eq. (20) is the usual Vandermonde factor on a torus, while the second term places q center-of-mass zeros at positions $\{\alpha_k\}$, k=1, ..., q. From now on we will enforce periodic boundary conditions by requiring that $\sum_k^q \alpha_k = 0 \mod L$. As already discussed in Section II, the $f(z)$ is the "modified Weierstrass sigma" function times Gaussian: $f(z) = \sigma(z)\exp -\frac{1}{2N_\phi} zz^*$. All model wavefunctions presented in this section are factorizable into a holomorphic function times a Gaussian factor $\prod_i \exp(-\frac{1}{2} z_i z_i^*)$.

Inserting additional N_h fluxes in the $\nu = 1/q$ Laughlin wavefunction creates quasi-hole excitations. The wavefunction with $\{w\}$ representing the positions of the quasiholes is,

$$\Psi(\{\alpha\},\{w\}) = \qquad (21)$$
$$\prod_{i<j}^{N_e} f^q(z_i - z_j) \prod_{i,a}^{N_e,N_h} f(z_i - w_a) \prod_{k=1}^{q} f(Z + \tfrac{W}{q} - \alpha_k).$$

In the following, we will use the Monte Carlo to calculate this Berry phase Φ. We take the one-hole model wavefunction $N_h = 1$, and move it around a path $w_0 \to w_1 \to ... \to w_{n-1} \to w_0$. At each step, we compute the overlap between the wavefunctions with $w = w_n$ and w_{n+1}. To compute the Berry phase, we take the product of these overlaps:

$$\langle\psi(w_0)|\psi(w_1)\rangle ... \langle\psi(w_{n-1})|\psi(w_n)\rangle = |D|e^{i\Phi}.$$

Since our numerics turns the continuous motion of the quasi-hole into a series of discrete steps, the amplitude $|D|$ will be smaller than one. The system has probability of $1-|D|$ jumping to the excited state and scrambling the phase. Therefore it is important to keep the step length $|w_i - w_{i+1}|$ small so that $|D|$ is close to one.

The numerical results for Laughlin $q = 3$ and $q = 5$ states are represented in (Fig. 1). We see that our observed values are what we expect them to be.

One can also do braiding of holes, or even more exotic anyons in other topological states [5, 6]. Here we just use a Laughlin hole as a trivial example to illustrate the Berry phase calculation.

B. CFL Berry Phase

The composite-Fermi-liquid state is a gapless state that forms at LL filling $\nu = 1/q$ when q is even. An emergent Fermi surface of composite fermion forms [12]. In this subsection, we will calculate the Berry phase acquired by moving one composite fermion around the Fermi surface.

There are some model wavefunctions proposed for the CFL state, such as $\det_{ij} e^{i\boldsymbol{d}_i\cdot\boldsymbol{R}_j}|\Psi_L^{\frac{1}{2}}\rangle$ [36, 37] where $|\Psi_L^{\frac{1}{2}}\rangle$ is the boson Laughlin state. Evaluating this wavefunction when projecting to a single LL unfortunately requires anti-symmetrization of $N_e!$ terms, and therefore quickly becomes unfeasible for practical calculation when

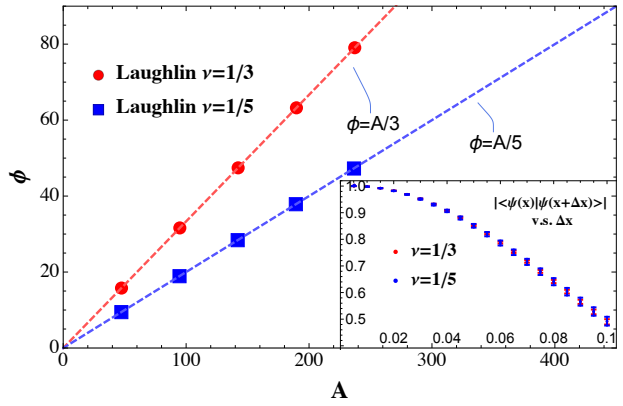

FIG. 1: $N_e = 50$, $\nu = 1/q$. Laughlin-hole state Berry phase (Φ) *v.s.* area the loop enclosed (A). The dot and the square show Monte-Carlo data for $q = 3$ and $q = 5$ respectively. The Monte-Carlo error is bounded by the line width. This demonstrates that $\Phi = A/q$. The inset shows the overlap $|\langle\psi(0)|\psi(\Delta x)\rangle|$ *v.s.* Δx which allows us to take step steplength to be $\Delta x = 0.02$ *i.e.* the quantum distance between consecutive steps is small.

N_e is large. In this work we consider instead the following model wavefunction [23, 24], whose computational complexity is $O(N_e^3)$.

$$\Psi_{CFL}(\{\alpha\},\{d\}) = \det \tilde{M}_{ij} \prod_{i<j} f^{q-2}(z_i - z_j) \prod_{k=1}^{q} f(Z - \alpha_k). \tag{22}$$

where $\tilde{M}_{ij}$ is a $N_e \times N_e$ matrix, and $\det \tilde{M}_{ij}$ is its determinant:

$$\tilde{M}_{ij} = e^{\frac{1}{2q}(z_i d_j^* - z_i^* d_j)} \prod_{k\neq i}^{N_e} f(z_i - z_k - d_j + \bar{d}).$$

In addition to a dependence on the q center of mass zeros $\{\alpha\}$, this wavefunction depends on N_e additional parameters $\{d\}$, the dipole moments. Like many quantum Hall wavefunctions, this wavefunction surrounds each electron with a "correlation hole": a region of depleted charge. In this wavefunction, the center of the correlation hole is displaced from the electron by d_j. In the magnetic field, a dipolar electron always moves perpendicular to its dipole direction, therefore the composite fermion's momentum is $k_a = l_B^{-2}\epsilon_{ab} e d^b$.

Requiring that all electrons see the same boundary conditions sets some constraints on the $\{d\}$. The zeros seen by the i^{th} particle add up to $\alpha - d + N_e d_{P(i)}$. Since all electrons must satisfy the same boundary condition, d_i must take $\{m\frac{L_1}{N_e} + n\frac{L_2}{N_e}\}$ values. Of course this quantization makes sense if we remember that $l_B^{-2}\epsilon_{ab} e d^b$ represents the composite fermion momentum, and momentum is quantized on torus.

A shift of $\bar{d}$ is a continuous symmetry of the model wavefunction, as we noticed recently. And we also found that the unnormalized model wavefunction vanishes identically when $\bar{d}$ approaches the center of Fermi sea, when (and only when) dipoles form an inversion-symmetric Fermi sea and the number of electrons is even. We believe this is related to the extra degeneracy in a particle-hole symmetric system with even number of electrons in the inversion symmetric many-body momentum sector, and might be related to the emergent Dirac cone that gives raise to the observed Z_2 Berry phase, as we will discuss in the below.

From the numerical work we have done at small system sizes [25], we know that the model wavefunction is very close to the Coulomb ground state when the dipoles are clustered, and becomes less close when more dipoles are excited out of Fermi sea. We first need to define what it means to take a composite fermion around the Fermi sea. In this work we consider a set of states obtained from dipole moments which form a compact Fermi sea, plus one additional dipole moment. We move this dipole moment on a path which encloses the Fermi sea. Alternatively we can remove a dipole moment to make a composite-hole and move it around on a path inside the Fermi sea. Because the many-body momentum $K = \sum_i^{N_e} d_i$, these states defines a path in the momentum space.

Since our system has translational invariance, states with different many-body momentum $K_1 \neq K_2$ are generally orthogonal $\langle\psi(K_1)|\psi(K_2)\rangle = 0$. We must insert an operator that makes this overlap non-vanishing. The natural choice of this operator is the guiding center density operator $\rho(\boldsymbol{d}) = \sum_i^{N_e} t_i(\boldsymbol{d})$ which satisfies the GMP algebra $[\rho(\boldsymbol{d}_1), \rho(\boldsymbol{d}_2)] = 2i \sin\frac{\boldsymbol{d}_1\times\boldsymbol{d}_2}{2l_B^2}\rho(\boldsymbol{d}_1 + \boldsymbol{d}_2)$. We thus define a the many-body K-space Berry phase, which is a generalization of the single body Brillouin zone Berry phase, as follows,

$$|D|e^{i\Phi} = Tr(\boldsymbol{\Gamma}_{1,2}\boldsymbol{\Gamma}_{2,3}...\boldsymbol{\Gamma}_{\boldsymbol{N},\boldsymbol{1}}), \tag{23}$$

where for each step $(\boldsymbol{\Gamma}_{1,2})_{\alpha,\beta} \equiv \langle\psi_{1\alpha}|\rho(\Delta K_{12})|\psi_{2\beta}\rangle$ where ΔK_{12} takes a value in the first Brillouin zone and $\Delta K_{12} = K_1 - K_2 \mod L$. Here $\alpha, \beta = 0, 1$, labels the two-fold degenerate topological ground states. The off-diagonal elements of $\Gamma_{1,2}$ are small since they involve transition between different topological sectors.

From the exact diagonization study in [25], we have found that this phase is determined by the direction in which the composite fermion moves around the Fermi sea. The total phase is given by:

$$e^{i\Phi} = (i)^{N_+ - N_-}(-1)^{\eta}. \tag{24}$$

In the above formula, $(i)^{N_+-N_-}$ is a path-dependent phase, and $(-1)^{\eta}$ is the Z_2 part. N_+ (N_-) is the number of anti-clockwise (clockwise) steps, defined relative to the center of Fermi sea. Note that steps normal to the Fermi sea are not included, since they always have zero amplitude. The $\eta \in \mathbb{Z}$ is the winding number, that counts how many times the total path enclose the center of the Fermi sea. The observed Z_2 phase is consistent with the

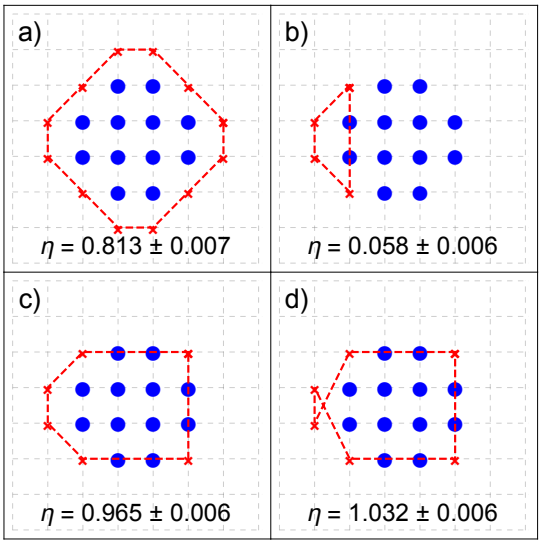

FIG. 2: $N_e = 13$ CFL Berry phase. Cross mark "x" represents the "composite fermion" we are moving. This is a consistency check with the same calculation done in [25] (but using a different numerical approach). This data can be interpreted through Eq.(24), which shows that in addition to a $\mathbb{Z}_2$ piece there is a piece depending on the direction of motion around the Fermi surface. When this is accounted for we find a residual "-1" from the $\mathbb{Z}_2$ part whenever the composite fermion encloses the Fermi sea.

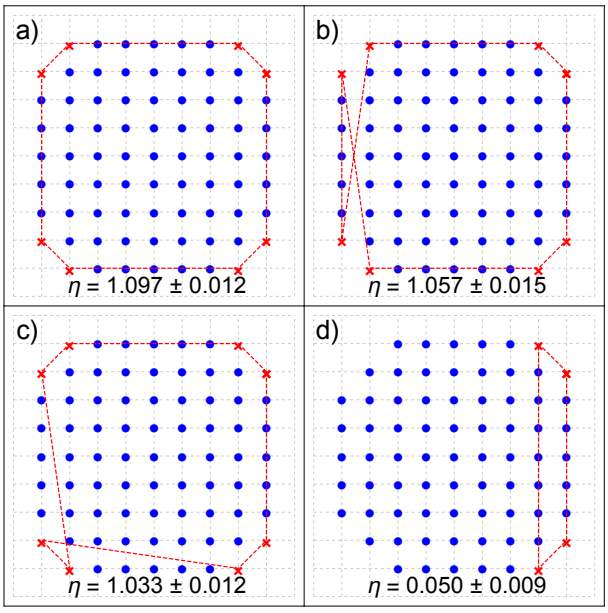

FIG. 3: $N_e = 69$ CFL Berry Phase. Cross mark "x" represents the "composite fermions" we are moving. The results are again consistent with Eq. (24)

low energy effective theory proposed in [20] where composite fermions are conjectured to be Dirac fermions and Berry flux is thus concentrated in the center of Fermi sea. More discussions on the many body Berry phase as well as exact numerical studies up to $N_e = 13$ electrons are given in [25].

The Monte Carlo calculation enables us to look at the Berry phase at much larger sizes, up to $N_e = 69$, and lets us check the Berry phase in a more convincing way. The following (Fig. 2) is done for $N_e = 13$, and (Fig. 3) is for $N_e = 69$. The results agree with Eq. (24), confirming that a $\mathbb{Z}_2$ phase is indeed obtained when composite fermions encircle the origin. Note that the model wavefunction Eq. (22) is not exactly particle-hole symmetric, therefore the observed Berry phase obtained using it is not exact, but is close to Z_2 phase.

IV. STRUCTURE FACTOR AND PAIR AMPLITUDE

Another application of the Monte Carlo technique is the (static) guiding center structure factor $S(\boldsymbol{q})$ which plays an important role in the FQH.

In the "single-mode approximation" first introduced by Feynman in superfluid Helium-4 [38] and then adopted by Girvin, MacDonald and Platzman in the FQH [39, 40], the structure factor provides a variational upper bound of the neutral excitation gap. In particular, the $|\boldsymbol{q}l_B| \to 0$ behavior of $S(\boldsymbol{q})$ is closely related to the collective modes in the system, and gives a criterion for the system to be gapped or gapless at long wavelength. For example, in superfluid Helium-4, $S(\boldsymbol{q}) \sim |\boldsymbol{q}l_B|^2$, corresponds to the gapless phonon mode, while in FQH $S(\boldsymbol{q}) \sim |\boldsymbol{q}l_B|^4$ corresponds to the gapped "graviton" mode [26]. For the Laughlin wavefunction, the 4^{th}- and 6^{th}- order expansion coefficients of $S(\boldsymbol{q})$ are predicted in [41]. The larger sizes accessible using our Monte Carlo method allow us to test these predictions.

Additionally, for the gapless CFL state, the peak in the structure factor can be used to identify the composite fermion Fermi surface, and identify its symmetry properties [21]. We can observe this physics in our Monte Carlo data. Lastly, from the structure factor, we found a method to greatly improve the Monte Carlo efficiency.

A. Structure Factor

The guiding center (static) structure factor by definition is the density-density correlation function,

$$S(\boldsymbol{q}) \equiv \frac{1}{2N_\phi}\langle\psi^{GC}|\{\delta\rho(\boldsymbol{q}), \delta\rho(-\boldsymbol{q})\}|\psi^{GC}\rangle. \quad (25)$$

where $\delta\rho(\boldsymbol{q})$ is the fluctuation of density operator $\rho(\boldsymbol{q})$ relative to the background $\langle\rho(\boldsymbol{q})\rangle/N_\phi = 2\pi l_B^2\nu\delta^2(\boldsymbol{q})$,

$$\rho(\boldsymbol{q}) = \sum_i^{N_e} e^{iq_aR_i^a},$$
$$\delta\rho(\boldsymbol{q}) = \rho(\boldsymbol{q}) - \langle\rho(\boldsymbol{q})\rangle. \quad (26)$$

Note that both $\delta\rho(\boldsymbol{q})$ and $\rho(\boldsymbol{q})$ satisfy the GMP algebra. Several properties of $S(\boldsymbol{q})$ are worth mentioning [42]. First, the large-$|\boldsymbol{q}l_B|$ asymptotic value is determined by the filling fraction $S(\infty)=\nu(1+\xi\nu)$, where $\xi=-1$ if the underlying particles are fermions, $=1$ if bosons. Second, $S(\boldsymbol{q})$ is self-dual under a Fourier transformation [42],

$$S(\boldsymbol{q})-S(\infty)=\xi\int\frac{d^2\boldsymbol{q}'l_B^2}{2\pi}e^{i\boldsymbol{q}\times\boldsymbol{q}'l_B^2}(S(\boldsymbol{q}')-S(\infty)). \tag{27}$$

Third, the coefficients of the small-$|\boldsymbol{q}l_B|$ expansion

$$S(|\boldsymbol{q}|)=c_2|\boldsymbol{q}l_B|^2+c_4|\boldsymbol{q}l_B|^4+c_6|\boldsymbol{q}l_B|^6+..., \tag{28}$$

contains useful information. For a gapped system, $c_2=0$. For a gapless system, $S(|\boldsymbol{q}|)$ goes to zero more slowly than $|\boldsymbol{q}l_B|^4$. For a Laughlin $\nu=1/q$ state, $c_2=0$, and predictions exist for c_4 and c_6 [41]:

$$\begin{aligned}c_4&=\frac{\nu|s|}{4},\\ c_6&=\frac{\nu|s|}{8}(s-\frac{c-\nu}{12}\frac{1}{\nu s}).\end{aligned} \tag{29}$$

where $s=-\frac{1}{2}(q-1)$ is the guiding center spin [26], c is the central charge. Our Monte Carlo method allows us to test these predictions (Fig. 4).

Another way to write Eq. (25) is the following,

$$S(\boldsymbol{q})=\frac{1}{N_\phi}\sum_{i,j}^{N_e}\langle\psi^{GC}|e^{i\boldsymbol{q}\cdot(\boldsymbol{R}_i-\boldsymbol{R}_j)}|\psi^{GC}\rangle-\frac{1}{N_\phi}\langle\rho(\boldsymbol{q})\rangle\langle\rho(-\boldsymbol{q})\rangle.$$

Writing $S(\boldsymbol{q})$ in this way reveals a challenge when computing it with our Monte Carlo method, which computes expectation values relative to the real-space coordinates r and Schrödinger wavefunctions rather than the guiding center versions. What our Monte Carlo calculates is the "full structure factor" (per flux), defined as:

$$S^{full}(\boldsymbol{q})=\frac{1}{N_\phi}\sum_{i,j}^{N_e}\langle\psi_0|e^{i\boldsymbol{q}\cdot(\boldsymbol{r}_i-\boldsymbol{r}_j)}|\psi_0\rangle_{Lat}-\frac{1}{N_\phi}\langle\rho(\boldsymbol{q})\rangle\langle\rho(-\boldsymbol{q})\rangle \tag{30}$$

We can relate these two quantities by using the form factor to simplify $S^{full}(\boldsymbol{q})$. This shows that $S^{full}(\boldsymbol{q})$ is related to the guiding center structure factor $S(\boldsymbol{q})$ via,

$$S^{full}(\boldsymbol{q})-\nu=|[f_0(\boldsymbol{q})]_{N_\phi}|^2\cdot[S(\boldsymbol{q})-\nu]. \tag{31}$$

The ν in the above equation comes from the terms in the sum where $i=j$. Because of the Gaussian function $f_0(\boldsymbol{q})=e^{-\frac{1}{4}\boldsymbol{q}^2l_B^2}$, the Monte Carlo error in $S(\boldsymbol{q})$ is amplified greatly when $|\boldsymbol{q}l_B|$ is large. This limits us to see the $S(\boldsymbol{q})$ within a window of small $|\boldsymbol{q}l_B|$. For Laughlin, $|\boldsymbol{q}_{max}|\approx 3l_B^{-1}$ (Fig. 4).

For the CFL states, the shape of the Fermi surface can be seen from the peak of structure factors. And the radius of the latter should be twice as large as that of the former. Here we plot the structure factor for model wavefunctions with different dipole-moment configurations for $N_e=37$ electrons (Fig. 5).

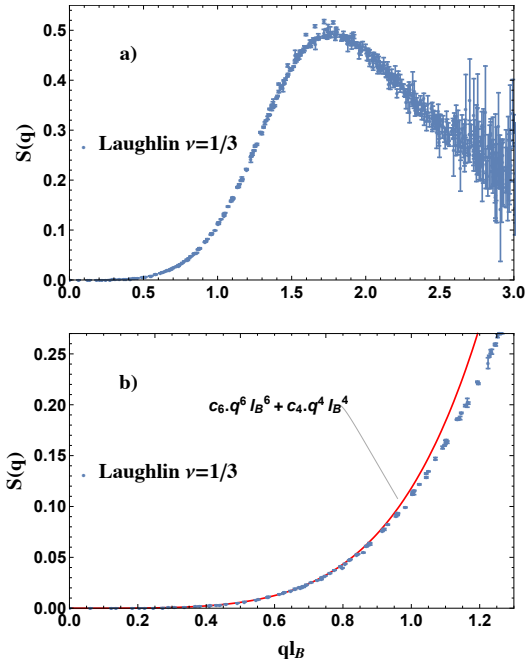

FIG. 4: The guiding center structure factor for $N_e=50$ electrons in the Laughlin $\nu=1/3$ state. The subfigure a) shows its plot together with error bars. The Gaussian function $e^{-\frac{1}{4}\boldsymbol{q}^2l_B^2}$ limits us to see $S(\boldsymbol{q})$ only within a window. In subfigure b), we check the long-wavelength expansion (c_4 and c_6) in (28) by comparing it to the Monte Carlo data, where c_4, c_6 is given by (29) and all other $c_i=0$. It can be seen that the long-wavelength behavior of $S(\boldsymbol{q})$ is correctly described by (29).

B. Improved Monte Carlo Algorithm

In Section II, we showed how to calculate any two-body expectation value $O(\boldsymbol{x}_i-\boldsymbol{x}_j)$, in any LL, and to demonstrate our method we computed the Coulomb energy of the Laughlin state in the first two LLs. However we found that for higher LLs (n>1), our method was subject to large Monte Carlo errors. In this section we will use our insights about the structure factor to understand and ameliorate these errors. The algorithm discussed in this section applies to other translational invariant two body interactions, like pair-amplitude. We will use the notation of Section II.

The first step in this process is to find out the effective potential acting on the guiding centers,

$$\begin{aligned}\langle\hat{O}\rangle&=\frac{1}{2\pi N_\phi}{\sum_{\boldsymbol{q}}}'\sum_{i<j}O^{GC}(\boldsymbol{q})\langle e^{i\boldsymbol{q}\cdot(\boldsymbol{R}_i-\boldsymbol{R}_j)}\rangle\\&=\frac{1}{4\pi N_\phi}{\sum_{\boldsymbol{q}}}'O^{GC}(\boldsymbol{q})\cdot[S(\boldsymbol{q})-\nu].\end{aligned} \tag{32}$$

In the problem of high LLs with index n, the Coulomb

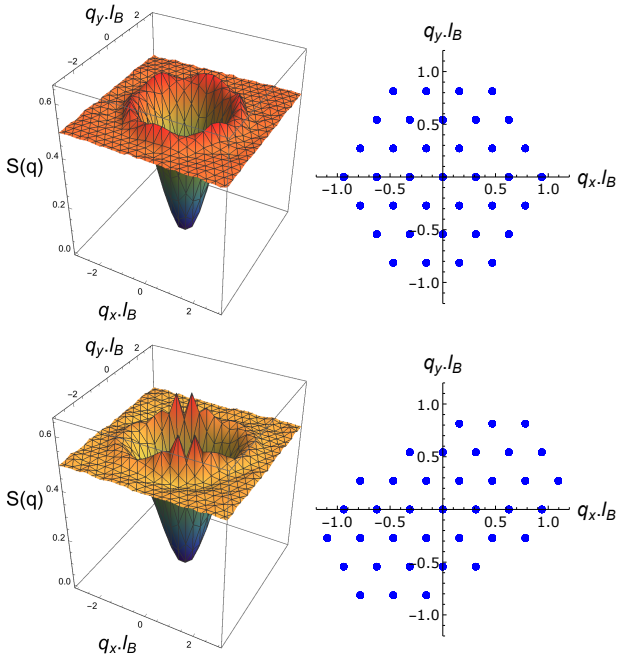

FIG. 5: CFL $S(\boldsymbol{q})$ and dipole configuration. The peak of the structure factor and composite fermion Fermi surface have the same shape. The radius of the former is twice of the latter.

energy is,

$$O^{GC}(\boldsymbol{q}) = [O(\boldsymbol{q}) f_n^2(\boldsymbol{q})]_c,$$
$$O(\boldsymbol{q}) = \frac{2\pi}{|\boldsymbol{q} l_B|}, \quad |\boldsymbol{q} l_B| \neq 0. \tag{33}$$

where the symbol $[...]^{GC}$ is defined in Eq. (16), not to be confused with $[...]_{N_\phi}$ defined in Eq. (18). Eq. (32) tells us that, at least in principle, the guiding center structure factor allows us to calculate any two-point expectation value. However, we found in the previous section that $S(\boldsymbol{q})$ determined from our Monte Carlo procedure has very large errors as at large $|\boldsymbol{q} l_B|$. The reason these errors do not completely ruin our calculation is that Eq. (32) also contains a form factor $f_n(\boldsymbol{q})$, which decays to 0 exponentially at large $|\boldsymbol{q} l_B|$, thus suppressing the errors. Unfortunately, the decay of $f_n(\boldsymbol{q})$ gets weaker as the LL index n is increased. This is why we we had difficulty calculating Coulomb energies for n>2 in Section II.

We can conclude that the large $|\boldsymbol{q} l_B|$ modes contribute a tiny amount to the mean value we want, and merely introduce large Monte Carlo error. Fortunately, Eq. (32) allows us to see a way to efficiently and accurately approximate $\langle \hat{O} \rangle$ since $S(\infty) = \nu(1-\nu)$ when $|\boldsymbol{q} l_B| \to \infty$ [1, 42]. We thus do the following trick: introduce a cutoff Q, and separate Eq. (32) into short-ranged ($|\boldsymbol{q}| > Q$) and long-ranged ($|\boldsymbol{q}| < Q$) parts. Only for the long-ranged part, we calculate by Monte Carlo by using the lattice representation Eq. (17). For the short-ranged part, we simply replace $S(\boldsymbol{q})$ with $S(\infty)$ and calculate *directly*.

$n = 2$, $Ql_B = 5$					
N_e	Exact	MC energy	δE_M	δE_S	δE_{tot}
4	−0.280537	−0.278	0.004	4e-4	0.004
5	−0.278052	−0.278	0.005	6e-4	0.005
6	−0.274849	−0.269	0.005	0.001	0.005
11	−0.268481	−0.271	0.006	0.001	0.006
12	−0.268005	−0.262	0.006	0.001	0.006

TABLE II: By separating the energy calculation into short- and long-ranged parts and approximating the long-ranged part, we can dramatically reduce our statistical error. In this table we compute the Coulomb energy of the Laughlin wavefunction in $n = 2$. We used the same number of Monte Carlo steps as we did in Table I, but find that our statistical error is reduced by up to two orders of magnitude even at these relatively small sizes. We also did test on larger systems, *e.g.* $N_e = 11, 12$.

Assuming that $S(\boldsymbol{q})$ is saturated when $|\boldsymbol{q}| > Q$ introduces systematic error δE_S. Although we do not know the short wavelength oscillation behavior of $S(\boldsymbol{q})$, we are still able to give an upper bound of $|\delta E_S|$, which could be calculated analytically. Note that $S(\boldsymbol{q})$ is positive and is bounded from above by its maximum value S_{max}, the oscillation must be less than $\min\{S^{max} - S(\infty), S(\infty)\}$. Hence, an upper bound of the systematic error is given by the following,

$$|\delta E_S| < \frac{1}{4\pi N_\phi} \sum_{|\boldsymbol{q}|>Q}{}' |O^{GC}(\boldsymbol{q})| \cdot \delta S \tag{34}$$
$$\delta S = \min\{S_{max} - S(\infty), S(\infty)\}.$$

From the plot of the structure factor Fig (4) and Fig (5), we empirically set $S_{max} \approx 0.5$ for the laughlin $\nu = 1/3$ state, $S_{max} \approx 0.8$ for CFL $\nu = 1/2$ state.

This systematic error δE_S must be included, together with the Monte Carlo error δE_M, into the total uncertainty $\delta E_{tot} = \sqrt{\delta E_M^2 + \delta E_S^2}$. Increasing the cutoff Ql_B decreases δE_S but makes δE_M larger. The best value of Ql_B is taken as the one for which δE_M and δE_S are of the same order.

Table II uses this approach to recalculate the Coulomb energies which were originally calculated in Table I. We can see that by cutting-off and approximating the large q contribution, we can significantly decrease the statistical error, and obtain improved estimates for the energy.

C. Pair Amplitudes

The self duality relation in Eq. (27) implies the $S(\boldsymbol{q})$ can be expanded in terms of Laguerre polynomials (multiplied by Gaussians), which form a complete basis of polynomials that are self-dual under Fourier transformations. The expansion coefficients in this basis are known as "pair amplitudes". Such pair-amplitudes appear in

the pseudo-potential Hamiltonian, and therefore it is interesting to ask whether they can be calculated in our Monte Carlo method.

Before defining pair-amplitudes on the torus, let us first look at the infinite plane geometry, where the pair-amplitude is better understood. The infinite plane has rotational symmetry, and angular momentum is well defined. A projector that projects a two-particle pair into a given state with relative angular momentum m is,

$$P_m^{ij} = 2\int \frac{d^2\boldsymbol{q} l_B^2}{2\pi} L_m(\boldsymbol{q}^2 l_B^2) e^{-\frac{1}{2}q^2 l_B^2} e^{i\boldsymbol{q}\cdot(\boldsymbol{R}_i - \boldsymbol{R}_j)}. \quad (35)$$

Here the P_m^{ij} are orthogonal projectors that satisfy,

$$P_m^{ij} P_m^{ij} = P_m^{ij}, \quad (36)$$
$$P_m^{ij} P_n^{ij} = 0, \quad \text{if } m \neq n. \quad (37)$$

The m^{th} pair-amplitude ξ_m is the probability of finding a pair of particles with relative angular momentum m,

$$\xi_m \equiv \langle \sum_{i<j} P_m^{ij} \rangle. \quad (38)$$

On the torus, P_m^{ij} is defined similarly as in Eq. (35), but with the integral over a continuum of momenta replaced by a discrete sum over all points in the reciprocal space. Since the torus does not have continuous rotation symmetry, the m does not have the meaning of "relative angular momentum" any more, and P_m^{ij} are no longer orthogonal: (37) does not hold, while (36) is modified

$$P_m^{ij} P_m^{ij} = C_m P_m^{ij}, \quad (39)$$

where C_m is a number that is slightly larger than one. The fact that (39) does not introduce any projectors with $m \neq n$ ensures that the torus Laughlin wavefunction is still the exact ground state of the pseudo-potential Hamiltonian. Although the torus has only discrete rotation symmetry, the continuous rotation symmetry is restored and the P_m^{ij} become orthogonal ($C_m \to 1$) in the limit $N_\phi \to \infty$.

The calculation of pair-amplitudes is similar in spirit to that of the Coulomb energy in high-index LLs. In the problem of calculating the pair-amplitude, we simply replace Eq. (33) with Eq. (40). The error analysis follows the same algorithm as discussed in the last section. This time,

$$O^{GC}(\boldsymbol{q}) = 4\pi [L_m(\boldsymbol{q}^2 l_B^2) e^{-\frac{1}{2}\boldsymbol{q}^2 l_B^2}]_c \quad (40)$$

In Table III, we showed several orders of calculated pair-amplitudes for Laughlin $\nu = 1/3$ state for $N_e = 6$ particles.

V. PARTICLE-HOLE OVERLAP THROUGH MONTE-CARLO

It is interesting to ask how close wavefunctions such as Eq. (22) are to having particle-hole symmetry. In [25], we have addressed this question by numerically second-quantizing these wavefunctions, and then implementing particle-hole symmetry in the second-quantized basis by exchanging the filled and empty orbitals. Since we have now developed a tool for rapid calculations in the Schrödinger representation, it is natural to ask whether we can evaluate particle-hole symmetry in this representation.

	ED	MC Value	Ql_B	δE_M	δE_S	δE_{tot}
ξ_1	0.	1e-3	5.00	1e-3	5e-4	1e-3
ξ_3	5.928056	5.84	5.00	0.08	0.04	0.09
ξ_5	4.441078	3.75	5.00	0.8	0.7	1.08

TABLE III: The pair-amplitude calculated for $N_e = 6$ particles in Laughlin $\nu = 1/3$ state. The δE_M and δE_S are Monte Carlo error and systematic error respectively. The total error $\delta E_{tot} = \sqrt{\delta E_M^2 + \delta E_S^2}$.

According to [43], if we have some wavefunction Ψ_1, we can compute its particle-hole conjugate as follows:

$$\Psi_1^{PH}(\tilde{z}_j) = \int \prod_{i=1}^{N_e} dz_i \ \Psi_1(z_i) \Psi_{LL}^*(z_i, \tilde{z}_j) \quad (41)$$

where Ψ_{LL} is the wavefunction for a filled LL. Using this definition of particle-hole conjugation we can compute the quantity $\langle \Psi_{CFL}^{\beta}(\{d\}) | PH \ \Psi_{CFL}^{\beta'}(-\{d\}) \rangle$, which is the overlap between the CFL state and its particle-hole conjugate. Here β indicates which center-of-mass sector the wavefunction is in, while $\{d\}$ represents the set of composite fermion dipole-moments of the wavefunction. Particle-hole symmetry on its own changes the momentum of a wavefunction, so when we write PH we really mean particle-hole symmetry combined with a rotation by π, an operation which preserves the symmetry [25]. The π-rotation reverses the center-of-mass sector (so we will need $\beta \neq \beta'$), and also takes $d \to -d$. Equivalently to reversing the d's, we can instead reverse all the coordinates z, which is what we will do from now on. Using Eq. (41), we can write the particle-hole overlap as follows:

$$\langle \Psi_{CFL}^{\beta}(\{d\}) | PH \ \Psi_{CFL}^{\beta'}(-\{d\}) \rangle = \quad (42)$$
$$\int \prod_{j=N_e+1}^{N_\Phi} d\tilde{z}_j \Psi_{CFL}^{\beta}(\{\tilde{z}_j\}) \times$$
$$\int \prod_{i=1}^{N_e} dz_i \ \ \Psi_{CFL}^{\beta'}(-\{z_i\}) \Psi_{LL}^*(\{z_i\}, \{\tilde{z}_j\})$$
$$= \langle \psi_1(x) | \psi_2(x) \rangle$$
$$\psi_1(x) = \Psi_{CFL}^{\beta}(\{z_j\}) \Psi_{CFL}^{\beta'}(-\{z_i\}) \quad (43)$$
$$\psi_2(x) = \Psi_{LL}^*(\{z_i\}, \{\tilde{z}_j\}) \quad (44)$$

In the above equation we have stopped explicity writing the variational parameters $\{d\}$, and as in Sec. (II) we use x as a shorthand for all the coordinates $\{z_i\}, \{\tilde{z}_j\}$.

In Sec. (II), [specifically Eq. (19)] we were calculating the overlap $\langle \psi_1 | \psi_2 \rangle$ and we manipulated the wavefunc-

tions in such a way that $|\psi_1|^2$ could be used as a Metropolis weight. However, we could in principle use any real, non-negative function as a weight. This inspires a more general version of Eq. (19):

$$\frac{\langle\psi_1|\psi_2\rangle}{\sqrt{\langle\psi_1|\psi_1\rangle\langle\psi_2|\psi_2\rangle}} = \frac{\sum' O_{12}(\boldsymbol{x})p(\boldsymbol{x})}{\sqrt{[\sum' O_{11}(\boldsymbol{x})p(\boldsymbol{x})][\sum' O_{22}(\boldsymbol{x})p(\boldsymbol{x})]}}. \tag{45}$$

where $O_{ij}(\boldsymbol{x}) \equiv \frac{\psi_i^*(\boldsymbol{x})\psi_j(\boldsymbol{x})}{p(\boldsymbol{x})}$. Here $p(\boldsymbol{x})$ is the statistical weight, so it must be real and non-negative. $|\psi_1|^2$ is a good choice for $p(\boldsymbol{x})$ when ψ_1 and ψ_2 are very similar, because it means that $O(\boldsymbol{x})$ will be of order one, and this is necessary for efficient importance sampling. If $O(\boldsymbol{x})$ can vary widely, then we will no longer be doing importance sampling (*i.e.* configurations where $O(\boldsymbol{x})p(\boldsymbol{x})$ is large will not be sampled frequently) and the algorithm will be inefficient. If $p(\boldsymbol{x}) = 0$ when $\psi_1(\boldsymbol{x})$ [or $\psi_2(\boldsymbol{x})$] is non-zero the Monte Carlo will give incorrect results since $O_{11}(\boldsymbol{x})$ [or $O_{22}(\boldsymbol{x})$] is infinite.

The ψ_1 and ψ_2 defined in Eqs. (43-44) are not very similar, and in fact one can have zeros where the other one is large. A simple way to see this is that whenever z_i=$\tilde{z}_j$ for any i, j in Eq. (42), ψ_2 will vanish but ψ_1 does not have to. Therefore simply using $|\psi_1|^2$ or $|\psi_2|^2$ for $p(\boldsymbol{x})$ will not work. In this work we make the following choice for $p(\boldsymbol{x})$:

$$p(\boldsymbol{x}) = (\alpha|\psi_1(\boldsymbol{x})| + |\psi_2(\boldsymbol{x})|)^2. \tag{46}$$

The virtue of this choice is that $p(\boldsymbol{x})$ will be large whever either ψ_1 or ψ_2 is large. The CFL wavefunctions are not normalized so the parameter α is included to make the two terms in the sum have approximately equal size. Using a fixed value of α (*e.g.* $\alpha = 1$) will give correct results but tuning α for a given system size can dramatically improve the performance of the Monte Carlo. We find for the wavefunctions used in this paper that $|\psi_1(\boldsymbol{x})|^2$ is roughly two orders larger than that of $p(\boldsymbol{x})$. Note that other choices of $p(\boldsymbol{x})$ are possible so long as it is large whenever either wavefunction is large, it maybe be possible to further improve performance with a better choice of $p(\boldsymbol{x})$.

A final obstacle to computing the particle-hole overlap is that the wavefunctions produced by Eq. (41) are not normalized, even if the wavefunctions on the right-hand side of that equation are normalized. In order to obtain a normalized wavefunction (and therefore a sensible overlap) we need to multiply Eq. (41) and (42) by a normalization constant $\sqrt{C}$, where

$$C = \begin{pmatrix} N_\Phi \\ N_e \end{pmatrix}. \tag{47}$$

The value of this constant can be explained by thinking about the overlap we are calculating as an overlap of the wavefunctions ψ_1, ψ_2 defined in Eqs. (43-44). If the two CFL wavefunctions were particle-hole symmetric, this overlap would be 1. But wavefunction ψ_1 is completely antisymmetric under interchanging coordinates z_i (which appears in one CFL wavefunction) and $\tilde{z}_j$ (which appears in the other wavefunction). In order for the overlap to be 1, ψ_2 must therefore also have this symmetry, but it clearly does not. Therefore to get sensible results we must antisymmetrize Eq. (44). Each term in such an antisymmetrization will be exactly the same once all positions are summed over, but in order to stay normalized we must divide by the square root of the number of terms in the antisymmetrization, which is exactly $\sqrt{C}$.

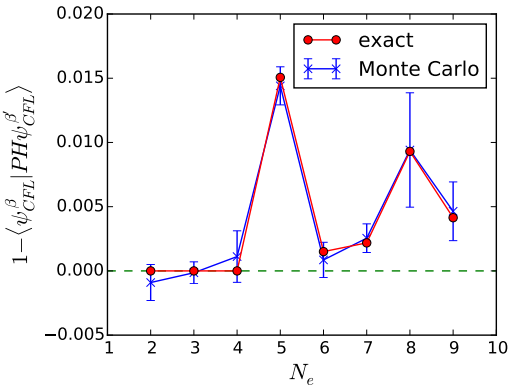

FIG. 6: Overlaps between a wavefunction and its PH conjugate. The red points from come from doing an exact second-quantization of the model wavefunction as in Ref. 25, while the blue comes from a Monte Carlo calculation. For each N_e, the configuration of d's with the largest overlap was used.

This normalization constant means both the values produced by numerically computing Eq. (45) *and their statistical errors* must be multiplied by $\sqrt{C}$. Therefore to keep the statistical errors constant in system size, the number of Monte Carlo steps requires scales as $\propto C$. This is the same algorithmic complexity as numerically second-quantizing the wavefunction, as in Ref. 25. Therefore there is no benefit to using our Monte Carlo method to compute particle-hole overlaps. Nevertheless the algorithm does work, as can be seen in Fig. 6 where we show the particle-hole overlaps for a few values of N_e, and compare them to the results of numerical second quantization. The $N_e = 9$ data in Fig. 6 took 600 CPU hours, while doing the exact second-quantizing algorithm takes around ten minutes. Therefore though using Monte Carlo does give correct results, it is not a practical method to evaluate the particle-hole symmetry of model wavefunctions.

VI. DISCUSSION

We have shown that quantum Hall problems on a torus in a single Landau level supports a discretized Lattice representation. This procedure can be used to dramatically save the time required for Monte Carlo calculations, because the continuous sampling is redundant and

the special functions required for quantum Hall wavefunctions on a torus can be tabulated in advance. We used our procedure to calculate a number of quantities, such as the energy of model wavefunctions, quasiparticle braiding statistics, the Berry phase acquired by composite fermions moving around the composite Fermi surface, guiding center structure factors and the particle-hole symmetry of model wavefunctions. Our Monte Carlo confirmed that the CFL at half filling has a Z_2 Berry phase factor at much larger system sizes than that in [25], and is consistent with the Dirac fermion effective theory [20] prediction.

During the time when this work was under review, several related work came out. The Berry phase associated with transporting two composite fermions was studied in [35]. The effects of Landau level mixing on the many-body Berry phase were studied in [44]. Recently, the CFL Berry phase at $\nu = 1/4$ was calculated in [45]. Motived by it, a Dirac-type effective theory was proposed in [45], which generalizes Son's theory from half filling to all other filling fractions that CFL can occur. Similar theories were studied from a different but complementary perspective in [46].

Our method can be used to dramatically increase the accessible system sizes for almost every quantity calculated using Monte Carlo. There are a few quantities which we still do not know how to calculate, for example the real-space entanglement entropy. Applying our formalism to such methods is an interesting direction for future work.

ACKNOWLEDGMENTS

This work was supported by Department of Energy BES Grant DE-SC0002140.

APPENDIX: LATTICE REPRESENTATION FOR TWO-BODY OPERATORS

In this section, we derive the lattice representation of translationally invariant two-body operators, which is used above in Eq. (17). We will start with finding the lattice representation for one-body operators.

We will start by answering this question: given a periodic single body operator $O(\boldsymbol{x}) = O(\boldsymbol{x} + \boldsymbol{L})$, what is the corresponding lattice operator $O^{Lat}(\boldsymbol{x} \in \mathbb{L}/N_\phi)$ such that the continuous integral equals to the lattice summation (up to some constant C),

$$\langle\psi_1|\hat{O}|\psi_2\rangle = C\ \langle\psi_1|\hat{O}^{Lat}|\psi_2\rangle_{Lat} \tag{48}$$

where $\langle ...\rangle$ and $\langle ...\rangle_{Lat}$ represent the integral and lattice summation respectively.

Since $O(\boldsymbol{x})$ is periodic, its Fourier transform is,

$$O(\boldsymbol{x}) = \frac{1}{2\pi N_\phi}\sum_{\boldsymbol{q}} O(\boldsymbol{q})e^{i\boldsymbol{q}\cdot\boldsymbol{x}},$$
$$O(\boldsymbol{q}) = \int d^2\boldsymbol{x}\ O(\boldsymbol{x})e^{-i\boldsymbol{q}\cdot\boldsymbol{x}}. \tag{49}$$

The $O^{Lat}(\boldsymbol{x})$ is not only periodic but is defined on lattice. Its Fourier transform is,

$$O^{Lat}(\boldsymbol{x}) = \frac{1}{2\pi N_\phi}{\sum_{\boldsymbol{q}}}' O^{Lat}(\boldsymbol{q})e^{i\boldsymbol{q}\cdot\boldsymbol{x}},$$
$$O^{Lat}(\boldsymbol{q}) = \frac{2\pi}{N_\phi}{\sum_{\boldsymbol{x}}}' O^{Lat}(\boldsymbol{x})e^{-i\boldsymbol{q}\cdot\boldsymbol{x}}. \tag{50}$$

where $\sum'$ sums $\boldsymbol{q}$ in the first Brillouin zone. The resolutions of identity are: $\int d^2\boldsymbol{x}e^{i\boldsymbol{q}\cdot\boldsymbol{x}}=2\pi\delta_{\boldsymbol{q},\boldsymbol{0}}$, $\sum_{\boldsymbol{q}} e^{i\boldsymbol{q}\cdot\boldsymbol{x}}=2\pi N_\phi\delta(\boldsymbol{x})$, and $\frac{1}{N_\phi}\sum'_{\boldsymbol{q}'} e^{i\boldsymbol{q}\times\boldsymbol{q}'}=\delta_{\boldsymbol{q},\boldsymbol{0}}$, where $\delta_{\boldsymbol{q},\boldsymbol{0}}=N_\phi$ if $\boldsymbol{q}=\boldsymbol{0}$, $\delta_{\boldsymbol{q},\boldsymbol{0}}=0$ if otherwise. $\int d^2\boldsymbol{x}\delta(\boldsymbol{x})=1$.

In the same spirit as Section II, we can write the expectation value as follows,

$$\langle\psi_1|\hat{O}|\psi_2\rangle = \frac{1}{2\pi N_\phi}{\sum_{\boldsymbol{q}}}' O'(\boldsymbol{q})\langle\psi_1^{GC}|e^{i\boldsymbol{q}\cdot\boldsymbol{R}}|\psi_2^{GC}\rangle. \tag{51}$$

where $O'(\boldsymbol{q})$ is the operator defined only in the first Brillouin zone but it includes all other interactions exactly,

$$O'(\boldsymbol{q}) = \sum_{\boldsymbol{q}'} O(\boldsymbol{q}+\boldsymbol{q}'N_\phi)f_0(\boldsymbol{q}+\boldsymbol{q}'N_\phi). \tag{52}$$

where $f_0(q)$ is the lowest LL form factor Eq. (14). Since the form factor decays rapidly, when the system size is large $O'(\boldsymbol{q})$ is almost the same as $O(\boldsymbol{q})$ except at the Brillouin zone. Now take $O(\boldsymbol{x}) = e^{i\boldsymbol{q}\cdot\boldsymbol{x}}$. Eq. (51) and Eq. (49) then lead to the following equation,

$$\int d^2\boldsymbol{x}\ \psi_1^*(\boldsymbol{x})\psi_2(\boldsymbol{x})e^{i\boldsymbol{q}\cdot\boldsymbol{x}} = f_0(\boldsymbol{q})\langle\psi_1^{GC}|e^{i\boldsymbol{q}\cdot\boldsymbol{R}}|\psi_2^{GC}\rangle.$$

By Eq. (49), its inverse Fourier transformation is,

$$2\pi N_\phi\ \psi_1^*(\boldsymbol{x})\psi_2(\boldsymbol{x}) \tag{53}$$
$$= \sum_q f_0(\boldsymbol{q})e^{-i\boldsymbol{q}\cdot\boldsymbol{x}}\langle\psi_1^{GC}|e^{i\boldsymbol{q}\cdot\boldsymbol{R}}|\psi_2^{GC}\rangle.$$

Then, by using the same method that leads to Eq. (52), Eq. (53) can be compactified to the first Brillouin zone. But this time, we need to take into account the effect of the phase factor, which leads to a similar but different notion of compactification. The expression for this new compactification $[...]_{N_\phi}$ can be found in Eq. (18),

$$2\pi N_\phi\ \psi_1^*(\boldsymbol{x})\psi_2(\boldsymbol{x}) \tag{54}$$
$$= {\sum_{\boldsymbol{q}}}' [f_0(\boldsymbol{q})]_{N_\phi}e^{-i\boldsymbol{q}\cdot\boldsymbol{x}}\langle\psi_1^{GC}|e^{i\boldsymbol{q}\cdot\boldsymbol{R}}|\psi_2^{GC}\rangle.$$

Eq. (54) is the key identity. Based on it, and by using Eq. (50), we can easily derive,

$$\frac{2\pi}{N_\phi}\sum_{\boldsymbol{x}}{}' \psi_1^*(\boldsymbol{x})\psi_2(\boldsymbol{x})e^{i\boldsymbol{q}\cdot\boldsymbol{x}} = [f_0(\boldsymbol{q})]_{N_\phi}\langle\psi_1^{GC}|e^{i\boldsymbol{q}\cdot\boldsymbol{R}}|\psi_2^{GC}\rangle. \tag{55}$$

Taking $\boldsymbol{q}$=$\boldsymbol{0}$, in the limit $N_\phi \to \infty$, $[f_0(\boldsymbol{0})]_{N_\phi} \to 1$, the lattice sum is replaced by the integration $\frac{2\pi}{N_\phi}\sum_{\boldsymbol{x}}{}' \to \int d^2\boldsymbol{x}$ and we recover the orthogonality of wavefunctions [27].

The lattice inner product is then found to be,

$$\sum_{\boldsymbol{x}}{}' \psi_1^*(\boldsymbol{x})\psi_2(\boldsymbol{x})O^{Lat}(\boldsymbol{x}) \tag{56}$$
$$= \frac{1}{(2\pi)^2}\sum_{\boldsymbol{q}}{}' O^{Lat}(\boldsymbol{q})[f_0(\boldsymbol{q})]_{N_\phi}\langle\psi_1^{GC}|e^{i\boldsymbol{q}\cdot\boldsymbol{R}}|\psi_2^{GC}\rangle.$$

By comparing this to Eq. (51), the lattice representation for a single body operator is easily found to be $O^{Lat}(\boldsymbol{q}) = \frac{2\pi}{N_\phi}\frac{O'(\boldsymbol{q})}{[f_0(\boldsymbol{q})]_{N_\phi}}$.

The two-body operator is a straightforward generalization since,

$$\sum_{\boldsymbol{q},\boldsymbol{x}_i}{}' \psi_1^*(\boldsymbol{x}_1)\psi_2^*(\boldsymbol{x}_2)O^{Lat}(\boldsymbol{q})e^{iq(\boldsymbol{x}_1-\boldsymbol{x}_2)}\psi_3(\boldsymbol{x}_2)\psi_4(\boldsymbol{x}_1)$$
$$= \sum_{\boldsymbol{q},\boldsymbol{x}_i}{}' \psi_1^*(\boldsymbol{x}_1)\psi_4(\boldsymbol{x}_1)e^{i\boldsymbol{q}\cdot\boldsymbol{x}_1}[\psi_3^*(\boldsymbol{x}_2)\psi_2(\boldsymbol{x}_2)O^{Lat}(-\boldsymbol{q})e^{i\boldsymbol{q}\cdot\boldsymbol{x}_2}]^*.$$

Applying Eq. (54) or Eq. (55) twice, and comparing it with Eq. (15), we can solve the lattice representation for two-body operators, which is shown in Eq. (17).

[1] R. E. Prange and S. M. Girvin, *The Quantum Hall Effect* (Springer-Verlag, New York, 1987).
[2] R. B. Laughlin, Phys. Rev. Lett. **50**, 1395 (1983).
[3] R. Morf and B. I. Halperin, Phys. Rev. B. **33**, 2221 (1986).
[4] X. Zhu and S. G. Louie, Phys. Rev. Lett. **70**, 335 (1993).
[5] Y. Tserkovnyak and S. H. Simon, Phys. Rev. Lett. **90**, 016802 (2003).
[6] M. Baraban, G. Zikos, N. Bonesteel, and S. H. Simon, Phys. Rev. Lett. **103**, 076801 (2009).
[7] O. Ciftja, B. Cornelius, K. Brown, and E. Taylor, Phys. Rev. B **83**, 193101 (2011).
[8] J. Biddle, M. R. Peterson, and S. Das Sarma, Phys. Rev. B **87**, 235134 (2013).
[9] F. D. M. Haldane and E. H. Rezayi, Phys. Rev. B **31**, 2529 (1985).
[10] F. D. M. Haldane, Phys. Rev. Lett. **55**, 2095 (1985).
[11] F. D. M. Haldane, Journal of Mathematical Physics **59**, 081901 (2018), https://doi.org/10.1063/1.5046122.
[12] B. I. Halperin, P. A. Lee, and N. Read, Phys. Rev. B **47**, 7312 (1993).
[13] S. A. Kivelson, D.-H. Lee, Y. Krotov, and J. Gan, Phys. Rev. B **55**, 15552 (1997).
[14] D.-H. Lee, Phys. Rev. Lett. **80**, 4745 (1998).
[15] G. Murthy and R. Shankar, Rev. Mod. Phys. **75**, 1101 (2003).
[16] C. Wang, N. R. Cooper, B. Halperin, and A. Stern, Phys. Rev. X **7**, 031029 (2017).
[17] M. Mulligan, S. Raghu, and M. P. A. Fisher, Phys. Rev. B **94**, 075101 (2016).
[18] M. Barkeshli, M. Mulligan, and M. P. A. Fisher, Phys. Rev. B **92**, 165125 (2015).
[19] A. K. C. Cheung, S. Raghu, and M. Mulligan, Phys. Rev. B **95**, 235424 (2017).
[20] D. T. Son, Phys. Rev. X **5**, 031027 (2015).
[21] S. D. Geraedts, M. P. Zaletel, R. S. K. Mong, M. A. Metlitski, A. Vishwanath, and O. I. Motrunich, Science **352**, 197 (2016).
[22] J. K. Jain, Phys. Rev. Lett. **63**, 199 (1989).
[23] J. K. Jain and R. K. Kamilla, Phys. Rev. B **55**, R4895 (1997).
[24] J. Shao, E.-A. Kim, F. D. M. Haldane, and E. H. Rezayi, Phys. Rev. Lett. **114**, 206402 (2015).
[25] S. D. Geraedts, J. Wang, E. H. Rezayi, and F. D. M. Haldane, Phys. Rev. Lett. **121**, 147202 (2018).
[26] F. D. M. Haldane, Phys. Rev. Lett. **107**, 116801 (2011).
[27] F. D. M. Haldane, Journal of Mathematical Physics **59**, 071901 (2018).
[28] N. Metropolis, A. Rosenbluth, M. Rosenbluth, A. Teller, and E. Teller, J. Chem. Phys. **21**, 1087 (1953).
[29] W. K. Hastings, Biometrika **57**, 97 (1970).
[30] D. Yoshioka, Phys. Rev. B **29**, 6833 (1984).
[31] L. Bonsall and A. A. Maradudin, Phys. Rev. B **15**, 1959 (1977).
[32] D. F. Mross, J. Alicea, and O. I. Motrunich, Phys. Rev. X **7**, 041016 (2017).
[33] C. Wang and T. Senthil, Phys. Rev. B **93**, 085110 (2016).
[34] A. C. Balram and J. K. Jain, Phys. Rev. B **93**, 235152 (2016).
[35] M. Fremling, N. Moran, J. K. Slingerland, and S. H. Simon, Phys. Rev. B **97**, 035149 (2018).
[36] E. Rezayi and N. Read, Phys. Rev. Lett. **72**, 900 (1994).
[37] E. H. Rezayi and F. D. M. Haldane, Phys. Rev. Lett. **84**, 4685 (2000).
[38] R. P. Feynman, Statistical Mechanics, Chap. 11 (1972).

[39] S. M. Girvin, A. H. MacDonald, and P. M. Platzman, Phys. Rev. Lett. **54**, 581 (1985).
[40] S. M. Girvin, A. H. MacDonald, and P. M. Platzman, Phys. Rev. B. **33**, 2481 (1986).
[41] P. Kalinay, P. Markos, L. Samaj, and P. Travenec, J. Stat. Phys. **98**, 639 (2000).
[42] F. D. M. Haldane, arXiv e-prints , arXiv:1112.0990 (2011), arXiv:1112.0990 [cond-mat.str-el].
[43] S. M. Girvin, Phys. Rev. B. **29**, 6012 (1984).
[44] S. Pu, M. Fremling, and J. K. Jain, Phys. Rev. B **98**, 075304 (2018).
[45] J. Wang, arXiv e-prints , arXiv:1808.07529 (2018), arXiv:1808.07529 [cond-mat.mes-hall].
[46] H. Goldman and E. Fradkin, Phys. Rev. B **98**, 165137 (2018).